Competitive mechanism of *Γ*-*L* intervalley carrier transport and direct gap radiative recombination in GeSn alloys*

HUANG Shihao[1, 2, *], LI Hailin[1, 2], MAO Chenglong[1, 2], SUN Qinqin[1, 2], LI Qiongyu[1, 2], XIE Deng[1, 2]

1. Fujian Key Laboratory of Automotive Electronics and Electric Drive, Fujian University of Technology, Fuzhou 350118, China
2. School of Electronics, Electrical Engineering and Physics, Fujian University of Technology, Fuzhou 350118, China

Abstract

GeSn alloy, as a novel silicon-based optoelectronic material, exhibits significant application potential in the field of infrared photonics due to its tunable bandgap properties and compatibility with silicon-based CMOS processes. Although the experimental performance of GeSn laser under low-temperature conditions has been preliminarily validated, the optimization and practical application of this device still face challenges such as insufficient understanding of material properties. This work addresses issues such as the unclear carrier dynamics mechanisms in GeSn alloy applications in infrared photonics. A theoretical model integrating band parameters, non-equilibrium carrier transport, and radiative recombination is proposed to systematically investigate the mechanism by which thermal excitation and phonon-assisted processes influence the direct-band spontaneous emission in GeSn alloys under variable temperature conditions. The results indicate that the carrier transfer process between the Γ_{CBM} and L_{CBM} energy bands of GeSn alloy exhibits significant composition dependence: for low-Sn-content GeSn alloy with Sn content below 10%, temperature-induced $L_{CBM}\rightarrow\Gamma_{CBM}$ electron transfer dominates, leading to an increase in direct band emission efficiency with temperature rising, whereas in high-Sn-content GeSn alloys with Sn content between 10% and 20%, the $\Gamma_{CBM}\rightarrow L_{CBM}$ electron escape process is more pronounced, resulting in a decrease in direct band emission efficiency with the increase of temperature. A modified Arrhenius model of the carrier dynamics competition further indicates that thermal

---

* The paper is an English translated version of the original Chinese paper published in Acta Physica Sinica. Please cite the paper as: **HUANG Shihao , LI Hailin, MAO Chenglong, SUN Qinqin, LI Qiongyu, XIE Deng, Competitive mechanism of *Γ*-*L* intervalley carrier transport and direct gap radiative recombination in GeSn alloys.** *Acta Phys. Sin.*, 2026, 75(2): 020701. DOI: 10.7498/aps.75.20251050

excitation and phonon scattering synergistically regulate electron transfer between Γ_{CBM} and L_{CBM}. The analysis based on the modified Arrhenius model further indicates that both thermal excitation and phonon-assisted processes promote the injection and escape of electrons in the Γ_{CBM} valley, acting as key factors in modulating the radiative recombination efficiency at the direct bandgap of GeSn alloy. The red shift of the peak position in the spontaneous emission spectrum of GeSn alloy is mainly due to the bandgap contraction effect. At the same time, phonon-assisted processes reduce the dispersion of carrier energy distribution, leading to a pronounced narrowing effect in the direct band emission spectrum. The quantitative findings further elucidate the mechanism by which thermal excitation and phonon-assisted processes influence the direct bandgap luminescence of GeSn alloy, providing theoretical guidance for the performance regulation of infrared optoelectronic devices.

Keywords: GeSn alloys, thermal excitation, phonon assisted, direct band emission

doi:10.7498/aps.75.20251050

cstr: 32037.14.aps.74.20251050

1 Introduction

GeSn alloys represent an emerging functional material in silicon-based optoelectronics. Their technological significance stems from the band structure reconstruction induced by Sn incorporation. When the Sn composition ranges from 6% to 10%, the alloy undergoes a transition from an indirect to a direct bandgap, thereby enhancing radiative recombination efficiency and addressing the fundamental limitation of low luminescence efficiency in conventional silicon-based materials[1-5]. Moreover, the epitaxial growth process of this material is compatible with silicon-based CMOS technology[6], offering a viable pathway toward monolithic silicon photonic integration. Additionally, by tuning the Sn composition, the emission wavelength can be continuously tuned across the 2-5 μm spectral range[7], endowing the material with promising application potential in infrared optoelectronics.

Owing to the small energy separation between the conduction band minima (CBMs) at the Γ and L valleys in GeSn alloys, approximately 140 meV at 0% Sn composition, thermal excitation at finite temperatures provides the necessary energy for carriers to overcome the barrier between the L_{CBM} and Γ_{CBM} valleys during spontaneous emission[8]. Furthermore, phonon-assisted processes compensate for the momentum mismatch between these two valleys, thereby facilitating inter-valley carrier transfer

and modulating carrier distribution.

Recent theoretical calculations based on evolving band structures indicate that the energy difference between the L_{CBM} and Γ_{CBM} valleys progressively decreases with increasing Sn composition, laying a foundation for understanding thermally activated carrier transfer mechanisms[9]. Studies [10,11] have demonstrated that elevated temperatures promote thermal excitation of electrons from the L_{CBM} to the Γ_{CBM} in GeSn alloys, thereby enhancing the probability of direct-band radiative recombination. Reference [12] further reports that, at room temperature, electrons in the L_{CBM} can absorb intervalley optical phonons to transition into the Γ_{CBM}, effectively compensating for the momentum difference and significantly increasing the carrier population in the Γ_{CBM}. These thermally driven or phonon-assisted inter-valley carrier transfer processes provide a theoretical basis for interpreting the temperature-dependent characteristics of direct-band radiative recombination in GeSn alloys.

Experimentally, temperature-dependent photoluminescence (PL) measurements have been widely employed to analyze the temperature evolution of spontaneous emission intensity in GeSn alloys. Reference [13] reported variable temperature PL studies on $Ge_{0.997}Sn_{0.003}$ thin films, showing that within the 100-300 K range, the PL intensity associated with direct-band transitions monotonically decreases as temperature drops; below 100 K, the direct-band emission is completely quenched. In contrast, Reference [14] conducted steady-state PL experiments on high-Sn-composition GeSn samples (12% Sn) and systematically observed PL responses at different temperatures. The results revealed a pronounced decrease in PL intensity with rising temperature-behavior opposite to that observed in low-Sn-composition GeSn alloys. Reference [15] established a comprehensive phonon-assisted model for pure Ge, quantitatively evaluating the contributions of different phonon modes to the direct- and indirect-band PL spectra. Nevertheless, current research on GeSn alloys exhibits two notable limitations: (1) existing theoretical or experimental studies cannot accurately predict the luminescence efficiency trends of GeSn alloys with varying Sn compositions across a broad temperature range, as most findings focus on case studies of either fixed low- or high-Sn-composition samples; and (2) a quantitative correlation between evolving band structures and the dominant mechanisms of radiative recombination, governed by thermal excitation or phonon assistance, has not yet been established.

To address these issues, this study focuses on the carrier dynamics mechanisms critical for GeSn alloys in infrared photonic applications. By constructing a parameterized band structure model, non-equilibrium carrier transport equations, and a direct-band radiative recombination framework, we specifically elucidate how the synergistic effects of thermal excitation and phonon assistance modulate the

spontaneous emission characteristics of GeSn alloys under varying temperatures. The phenomenological model developed, the computational methodology adopted, and the quantitative data obtained in this work provide essential theoretical insights into the temperature-dependent optoelectronic properties of GeSn alloys.

2 Theoretical Model

2.1 Parameterized Band Structure Model

For GeSn alloys, the full Brillouin zone band structure can be calculated using a 30-band $k\,p$ perturbation theory[16]. The direct bandgap E_{g} as a function of Sn composition x and temperature T is given by the following expression[17,18]:

$$E_{\mathrm{g}}(x,T) = E_{\mathrm{g}}(x,0) - \frac{\alpha(x)T^2}{T+\beta(x)}, \quad (1)$$

In the equation, $E_{\mathrm{g}}(x,0), \alpha(x), \beta(x)$ represent, respectively,

$$\begin{aligned} E_{\mathrm{g}}(x,0) &= (2.871x^2 - 3.992x + 0.975)\mathrm{eV}, \\ \alpha(x) &= (9.914\mathrm{e}^{-1.5x} \times 10^{-4})\mathrm{eV/K}, \\ \beta(x) &= (236\mathrm{e}^{4x})\mathrm{K}. \end{aligned} \quad (2)$$

The electron and hole effective masses, m_{e} and m_{h}, of GeSn alloys can be obtained by fitting the parabolic nature of the *E*-*k* relationship[19]:

$$E_{\mathrm{C}}(k) = E_{\mathrm{C}}(0) + \frac{\hbar^2 k^2}{2m_{\mathrm{e}}}, \quad (3)$$

$$E_{\mathrm{V}}(k) = E_{\mathrm{V}}(0) - \frac{\hbar^2 k^2}{2m_{\mathrm{h}}}, \quad (4)$$

In the equation, $E_{\mathrm{C}}(k)$ denotes the conduction band electron energy, which can be divided into the direct band Γ_{CBM} and the indirect band L_{CBM}. The corresponding effective masses are $m_{\Gamma\mathrm{e}}$ and m_{Le}, respectively. $E_{\mathrm{V}}(k)$ represents the valence band electron energy. Additionally, the reduced effective mass m_{r} is defined by Equation (5):

$$\frac{1}{m_{\mathrm{r}}} = \frac{1}{m_{\mathrm{e}}} + \frac{1}{m_{\mathrm{h}}}. \quad (5)$$

2.2 Non-equilibrium Carrier Transport Model

Thermal excitation induced by temperature influences electron transfer in GeSn alloys

between the Γ_{CBM} and L_{CBM} valleys, thereby altering the electron distribution between these two valleys. Under thermal excitation, the electron concentrations in the Γ_{CBM} and L_{CBM} valleys are denoted by n_{Γ} and n_{L}, respectively. Their sum equals the total conduction band electron concentration n, as expressed by the following equation[20,21].

$$n = n_{\Gamma} + n_{L}, \quad (6)$$

Among these

$$n_{\Gamma} = \left[\frac{1}{2\pi^2}\left(\frac{2m_{\Gamma\mathrm{e}}k_{\mathrm{B}}T}{\hbar^2}\right)^{3/2}\right] \times \left[\int_0^{\infty} \frac{x^{1/2}\mathrm{d}x}{1+\exp\left(x-\xi+c\Delta E_{\Gamma L}/(k_{\mathrm{B}}T)\right)}\right], \quad (7)$$

$$n_{L} = \left[\frac{1}{2\pi^2}\left(\frac{2m_{\mathrm{Le}}k_{\mathrm{B}}T}{\hbar^2}\right)^{3/2}\right]\left[\int_0^{\infty} \frac{\mathrm{x}^{1/2}\mathrm{d}x}{1+\exp\left(x-\xi\right)}\right], \quad (8)$$

In the equation, k_{B} denotes the Boltzmann constant, T represents temperature, $\hbar$ is the reduced Planck constant, and $\Delta E_{\Gamma L}$ signifies the energy difference between Γ_{CBM} and L_{CBM}. $\xi = \frac{E_{\mathrm{FC}}-E_{\mathrm{C}}}{k_{\mathrm{B}}T}$. E_{C} and E_{V} denote the conduction band minimum and valence band maximum of the indirect bandgap, respectively. The quasi-Fermi levels for conduction band electrons (E_{FC}) and valence band holes (E_{FV}) are described by the Fermi-Dirac distribution functions $f_{\mathrm{C}}(E)$ and $f_{\mathrm{V}}(E)$, respectively:

$$f_{\mathrm{C}}(E) = \frac{1}{1+\exp\left(\frac{E-E_{\mathrm{FC}}}{k_{\mathrm{B}}T}\right)}, \quad (9)$$

$$f_{\mathrm{V}}(E) = \frac{1}{1+\exp\left(\frac{E_{\mathrm{FV}}-E}{k_{\mathrm{B}}T}\right)}. \quad (10)$$

The valence band hole concentration p can be expressed by the formula

$$p = \frac{1}{2\pi^2}\frac{(2k_{\mathrm{B}}Tm_{\mathrm{h}}^{*})^{2/3}}{\hbar^3}\int_0^{\infty} \frac{(x)^{1/2}}{1+\exp\left(x-\frac{E_{\mathrm{V}}-E_{\mathrm{FV}}}{k_{\mathrm{B}}T}\right)}\mathrm{d}x. \quad (11)$$

When accounting for phonon-assisted processes, the electron distribution between the Γ_{CBM} and L_{CBM} valleys under the influence of intervalley optical phonons can be described by Equation (12):

$$\frac{\mathrm{d}}{\mathrm{d}t}\begin{bmatrix} n_{\Gamma} \\ n_{\mathrm{L}} \end{bmatrix} = \begin{bmatrix} -R_{\Gamma\mathrm{L}} & R_{\mathrm{L}\Gamma} \\ R_{\Gamma\mathrm{L}} & -R_{\mathrm{L}\Gamma} \end{bmatrix}\begin{bmatrix} n_{\Gamma} \\ n_{\mathrm{L}} \end{bmatrix}. \quad (12)$$

In the matrix, $R_{\Gamma L}$ and $R_{L\Gamma}$ represent the intervalley optical phonon scattering rates from Γ_{CBM} to L_{CBM} and from L_{CBM} to Γ_{CBM}, respectively. Under the assistance of intervalley phonon scattering, nonequilibrium carriers undergo dynamic migration on the picosecond (ps) timescale and eventually reach steady-state equilibrium. Specific model parameters follow those established in our group's prior work[20]. It should be noted that in the GeSn alloy band structure, the conduction band minimum of the Δ valley lies at a higher energy than both Γ_{CBM} and L_{CBM}. Moreover, scattering among the three valleys-Γ_{CBM}, L_{CBM}, and Δ-introduces additional complexity. Consequently, this study reasonably neglects the contribution of electron populations in the Δ valley. A more accurate theoretical model would require explicit inclusion of the electronic states in the Δ valley.

2.3 Radiative Recombination Model

In GeSn alloys, spontaneous emission primarily arises from radiative recombination between conduction band electrons and valence band holes. The photon generation rate is described by the spontaneous emission rate $R_{sp}(\hbar\omega)$. Based on quantum mechanical perturbation theory, the spontaneous emission rate can be expressed as[22]

$$R_{sp}(\hbar\omega) = \frac{n_i \omega q^2}{\pi\hbar c^3 \varepsilon_0 m_0^2} \rho_{joint}(\hbar\omega - E_g) |\langle \boldsymbol{e} \cdot \boldsymbol{p} \rangle|^2 f_c (1 - f_v), \quad (13)$$

Here, n_i denotes the refractive index, ω represents the angular frequency of the emitted photon, q is the elementary charge, c is the speed of light in vacuum, ε_0 is the vacuum permittivity, m_0 is the free electron mass, ρ_{joint} is the joint density of states, and $\langle \boldsymbol{e} \cdot \boldsymbol{p} \rangle$ is the momentum matrix element. Equation (12) indicates that the spontaneous emission transition rate is proportional to the product of the conduction band electron occupation probability f_c and the valence band hole occupation probability (1 - f_v). The probabilities f_c and f_v are expressed as follows:

$$f_c = 1/[1 + \exp(\frac{E_1 - E_{FC}}{k_B T})], \quad (14)$$

$$f_v = 1/[1 + \exp(\frac{E_2 - E_{FV}}{k_B T})], \quad (15)$$

In the equation, when an electron with conduction band energy E_1 undergoes a direct band radiative transition to a state with valence band energy E_2, the emitted photon energy satisfies:

$$\hbar\omega = E_1 - E_2. \quad (16)$$

The joint density of states ρ_{joint} can be expressed as follows:

$$\rho_{\text{joint}}(\hbar\omega - E_{\text{g}}) = \frac{1}{2\pi^2}\left(\frac{2m_{\text{r}}^*}{\hbar^2}\right)^{3/2}(\hbar\omega - E_{\text{g}})^{1/2}. \quad (17)$$

The squared term of the momentum matrix can be further approximated as

$$|\langle \boldsymbol{e}\cdot\boldsymbol{p}\rangle|^2 = \left(\frac{m_0}{m_{\Gamma\text{e}}} - 1\right)\frac{m_0 E_{\text{g}}(E_{\text{g}}+\Delta)}{6(E_{\text{g}}+\frac{2}{3}\Delta)}, \quad (18)$$

Here, E_{g} denotes the direct bandgap width, and Δ represents the valence band splitting energy.

To obtain the total spontaneous emission rate R_{sp}, we integrate the emission rate per unit energy over the allowed energy range, yielding

$$R_{\text{sp}} = \int_{\hbar\omega_{\min}}^{\hbar\omega_{\max}} R(\hbar\omega)\mathrm{d}(\hbar\omega). \quad (19)$$

3 Results and Discussion

Under the thermal excitation model, Figure 1 presents the temperature-dependent spontaneous emission spectra of GeSn alloys with a direct bandgap ($\Gamma_{\text{CBM}}\rightarrow\Gamma_{\text{VBM}}$) at an injected carrier concentration of 1×10^{18} cm^{-3}. When the Sn composition is 5%, GeSn exhibits an indirect bandgap. As the temperature increases from 100 K to 300 K, the spontaneous emission intensity gradually rises. These computational results show good agreement with the photoluminescence (PL) data measured by Qian et al.[8] for samples with the same Sn composition over the 100-300 K temperature range. In contrast, when the Sn composition reaches 15%, GeSn becomes a direct bandgap material. Under this condition, the emission intensity progressively diminishes with increasing temperature, a trend that closely aligns with the temperature, dependent PL intensity behavior observed by Wirths et al.[23] in samples containing 12.6% Sn. Comparing the spontaneous emission intensities of direct- and indirect-bandgap GeSn alloys at the same temperature in Figures 1(a) and (b), we find that the $\Gamma_{\text{CBM}}\rightarrow\Gamma_{\text{VBM}}$ emission intensity of the indirect-bandgap GeSn alloy is significantly lower than that of the direct-bandgap counterpart. This occurs because, at an identical injected carrier concentration of 1×10^{18} cm^{-3}, a portion of the carriers in the indirect-bandgap GeSn alloy occupies the indirect L_{CBM} valley, thereby reducing the carrier population in the direct Γ_{CBM} valley and resulting in weaker luminescence intensity.

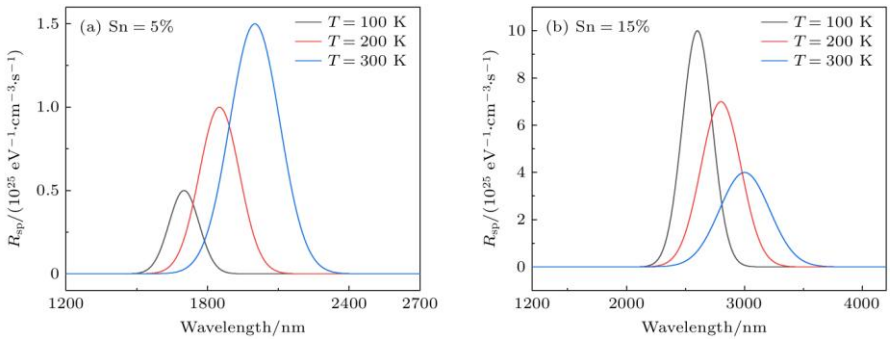

Fig. 1 Temperature-dependent spontaneous emission spectra of GeSn alloys under thermal excitation model at an injected carrier concentration of 1×10^{18} cm^{-3}: (a) Sn content of 5%; (b) Sn content of 15%.

To systematically elucidate the composition- and temperature-dependent characteristics of $\Gamma_{CBM}\rightarrow\Gamma_{VBM}$ radiative recombination dynamics in GeSn alloys, this study employed a radiative recombination model to compute a three-dimensional phase diagram depicting the variation of direct bandgap photoluminescence intensity at the Γ_{CBM} valley with composition and temperature, as shown in Figure 2.

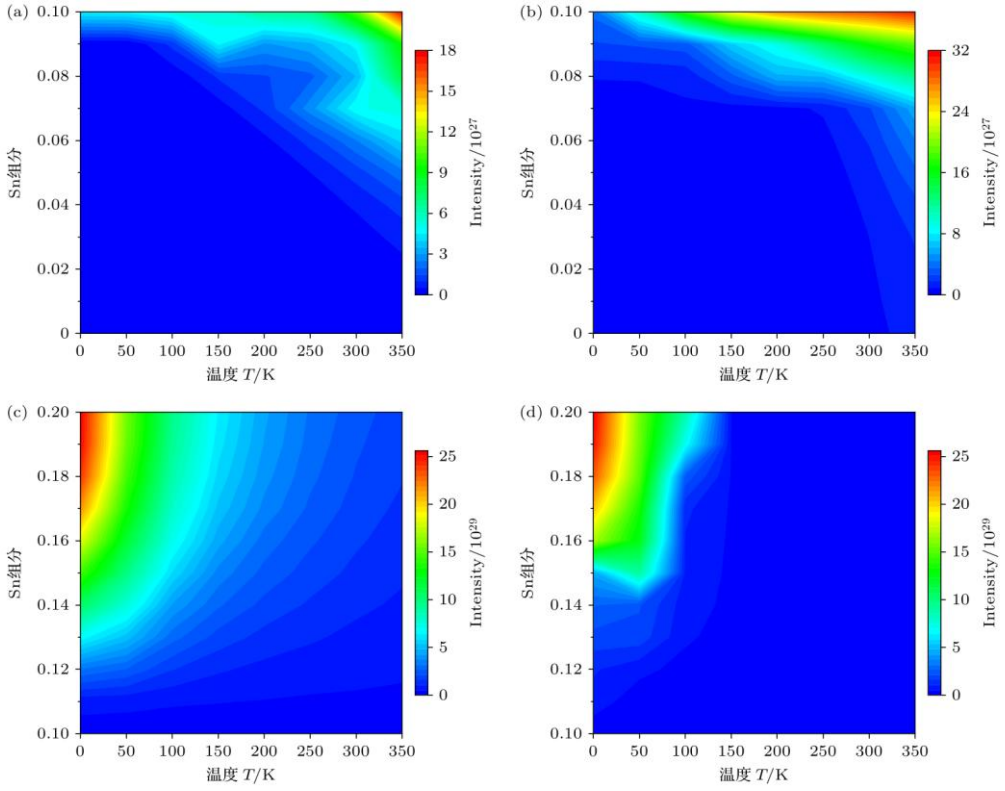

Fig. 2 Three-dimensional maps of direct bandgap emission intensity of GeSn alloys as a function of Sn content and temperature: (a) Thermal excitation model at low Sn content (*x* = 0–10%); (b) phonon-assisted model at low Sn content (*x* = 0–10%); (c) thermal excitation model at high Sn content (*x* = 10%–20%); (d) phonon-assisted model at high Sn content (*x* = 10%–20%).

For low-composition GeSn alloys with Sn fractions ranging from 0% to 10%, the model calculations in Fig. 2(a), which consider only thermal excitation, indicate that at a fixed temperature, increasing the Sn fraction enhances the direct-band emission intensity. Fig. 2(b) incorporates the phonon-assisted scattering process whereby carriers in the L_{CBM} valley scatter into the Γ_{CBM} valley. The results demonstrate that, at a fixed temperature, not only does the emission intensity of low-composition GeSn alloys increase with higher Sn fractions, but phonon participation also promotes greater electron occupation of the Γ_{CBM} valley, thereby enhancing the direct-band emission efficiency of GeSn alloys.

To visually illustrate the physical mechanism of phonon-assisted recombination, Fig. 3(a) presents a radiative recombination model for the indirect-bandgap $Ge_{0.95}Sn_{0.05}$ alloy at 100 K. In this figure, red/blue arrows (on the picosecond scale)[20] represent the phonon-driven inter-valley electron transition pathways, while black arrows (on the nanosecond scale)[24] denote the direct-band radiative recombination process. The calculations reveal that, at a fixed Sn fraction, elevated temperature enhances direct-band emission intensity. This behavior fundamentally arises because thermal excitation and phonon assistance increase the probability of electrons occupying the direct-band valley.

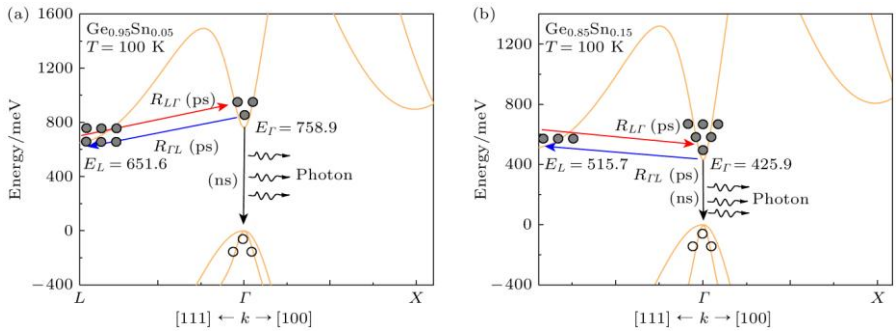

Fig. 3 Schematic diagram of phonon-assisted radiative recombination under different Sn compositions at 100 K: (a) 5% Sn composition; (b) 15% Sn composition.

The theoretical predictions align consistently with multiple experimental findings. For instance, Huang et al.[25] conducted temperature-dependent photoluminescence (PL) measurements on GeSn alloys with 3.1% Sn content over the 200-400 K temperature range, revealing a monotonic increase in PL intensity with rising temperature. Furthermore, Huang et al.[26] confirmed through room-temperature PL experiments that, within the low-composition range (x = 0.86%-7.8%), PL intensity increases with higher Sn composition. The agreement between these experimental results and theoretical predictions validates the physical mechanism underlying the synergistic modulation of GeSn alloy luminescence by temperature and composition.

For high-composition GeSn alloys with Sn content between 10% and 20%, the

computational results in Figures 2(c) and (d) demonstrate that, at a fixed temperature, the direct bandgap PL intensity from the Γ_{CBM} valley significantly increases with rising Sn composition-regardless of whether the thermal excitation model or the phonon-assisted recombination model is applied. However, at a fixed Sn composition, the direct bandgap PL intensity exhibits a pronounced decay trend as temperature increases, contrasting sharply with simulation results for low-composition GeSn alloys. As illustrated by the radiative recombination model for direct bandgap $Ge_{0.85}Sn_{0.15}$ alloy at 100 K in Figure 3(b), this phenomenon stems from the energy difference between the L_{CBM} and Γ_{CBM} valleys in high-composition GeSn alloys. With increasing temperature, thermal excitation enables more electrons to overcome the L_{CBM}-Γ_{CBM} energy barrier, while enhanced intervalley phonon-assisted processes further promote electron transfer from the Γ_{CBM} to the L_{CBM} valley. The synergistic effect of these two mechanisms substantially increases the carrier escape probability from the Γ_{CBM} to the L_{CBM} valley, thereby reducing radiative recombination efficiency in the Γ_{CBM} valley.

Three-dimensional phase diagram analysis of GeSn alloy PL intensity clearly reveals a nonlinear response of direct bandgap emission intensity to variations in both Sn composition and temperature. This dependence primarily arises from the interplay between competing thermal excitation and phonon-assisted mechanisms. To gain deeper insight into the underlying physics, this study systematically examines three key parameters of the spontaneous emission spectrum: first, the relationship between integrated intensity and temperature is analyzed to quantitatively determine the correlation between thermal or scattering activation energy and direct band radiative recombination efficiency; second, the dependence of spectral full width at half maximum (FWHM) on temperature is investigated to quantitatively characterize radiative carrier recombination and phonon-assisted non-radiative recombination processes; finally, spectral peak shifts are examined to directly reflect the influence of temperature on the bandgap of GeSn alloys.

In semiconductor material characterization, the Arrhenius equation serves as a classical kinetic model for thermally activated processes and provides a crucial theoretical framework for analyzing intervalley carrier transfer mechanisms[27]. In the GeSn system, this study reveals that intervalley carrier transfer exhibits pronounced composition dependence: in low-composition GeSn alloys, temperature-induced $L_{CBM} \rightarrow \Gamma_{CBM}$ electron transfer dominates, enhancing direct band emission efficiency; conversely, in high-composition GeSn alloys, $\Gamma_{CBM} \rightarrow L_{CBM}$ electron escape becomes more significant, reducing direct band emission efficiency. To quantitatively characterize these competing thermally activated processes, this work establishes a modified Arrhenius model:

$$I(T) = \frac{I_0}{1+A\cdot e^{\pm E_a/kT}}, \quad (20)$$

Here, I_0 denotes the integrated intensity at 0 K, A represents the empirical enhancement factor, k is the Boltzmann constant, and E_a signifies the activation energy required for thermal excitation or intervalley scattering. The positive (+) and negative (-) terms correspond to the intervalley injection into and escape from the direct-band Γ_{CBM} valley, respectively. Integrated intensity analysis of the temperature-dependent photoluminescence spectra shown in Figure 4 reveals excellent agreement between the data simulated by the thermal excitation and phonon-assisted models (solid dots) and the fitting curve generated by the modified Arrhenius model (solid line), thereby validating the effectiveness of the modified Arrhenius model in quantitatively determining the thermal activation energy and intervalley scattering activation energy in GeSn alloys.

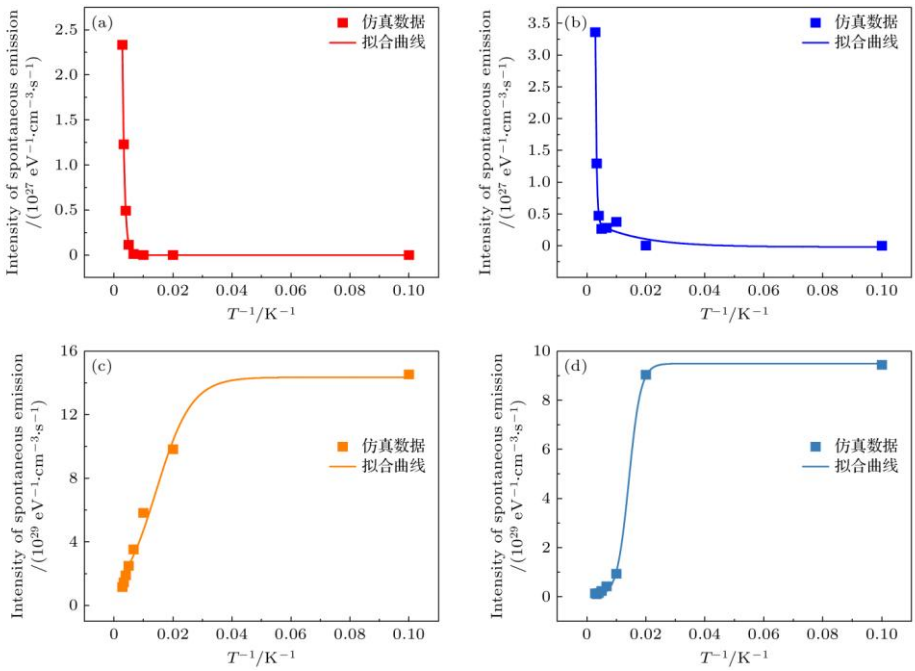

Fig. 4 Temperature-dependent integrated spontaneous emission intensity of GeSn alloys fitted with the modified Arrhenius model: (a) 5% Sn, thermal excitation model; (b) 5% Sn, phonon-assisted model; (c) 15% Sn, thermal excitation model; (d) 15% Sn, phonon-assisted model.

To systematically investigate the compositional dependence of scattering mechanisms in GeSn alloys, Figure 5 compares the evolution of activation energies derived from the thermal excitation model and the phonon-assisted model. The data reveal two key observations: First, under a fixed Sn composition, the difference in activation energies between the two models remains small, indicating that both thermal excitation and phonon assistance can facilitate electron injection into or escape from the Γ_{CBM} valley.

These processes represent critical factors that either enhance or suppress radiative recombination efficiency. Second, an Sn composition of 10% serves as a critical threshold. As the Sn content approaches 10%, the energy difference between the L_{CBM} and Γ_{CBM} valleys in GeSn alloys becomes minimal, resulting in the lowest activation energy. Consequently, electrons redistribute more readily between the L_{CBM} and Γ_{CBM} valleys, achieving equilibrium. Furthermore, the trend in activation energy provides additional insight into the dominant electron transfer mechanism: In the indirect bandgap regime with low Sn content, the relatively large activation energy reflects the substantial energy required for electrons to inject from the L_{CBM} valley into the Γ_{CBM} valley, thereby enhancing direct-band radiative emission. Conversely, in the direct bandgap regime with high Sn content, the increasing Sn composition enlarges the L_{CBM}-Γ_{CBM} energy separation, indicating that electrons require higher activation energy to escape the Γ_{CBM} valley and transition toward the indirect band, thus diminishing direct-band emission efficiency.

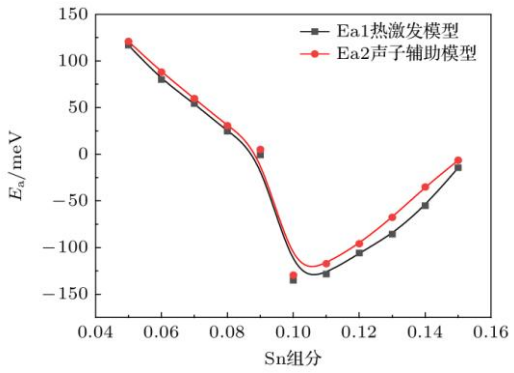

Fig. 5 Sn content dependence of extracted thermal activation energy (E_a) in GeSn alloys under thermal excitation and phonon-assisted models.

Figure 6 illustrates the temperature-dependent evolution of the full width at half maximum (FWHM) of the spontaneous emission spectra for GeSn alloys with varying Sn compositions. In both the thermal excitation model and the phonon-assisted model, the FWHM of all compositions increases monotonically with rising temperature. Moreover, the broadening in high-Sn-composition GeSn alloys is significantly greater than that in low-Sn-composition alloys. This behavior primarily arises because either elevated temperature or increased Sn composition narrows the bandgap of GeSn, thereby widening the energy distribution of electron-hole recombination and directly increasing the spectral FWHM. Additionally, under identical composition and temperature conditions, the FWHM predicted by the phonon-assisted model is smaller than that from the thermal excitation model. This reduction occurs because phonon participation enables directional carrier transport through specific phonon modes to satisfy momentum conservation, substantially decreasing the energy distribution dispersion of carriers. Notably, this phonon-assisted spectral narrowing effect

becomes particularly pronounced above 200 K.

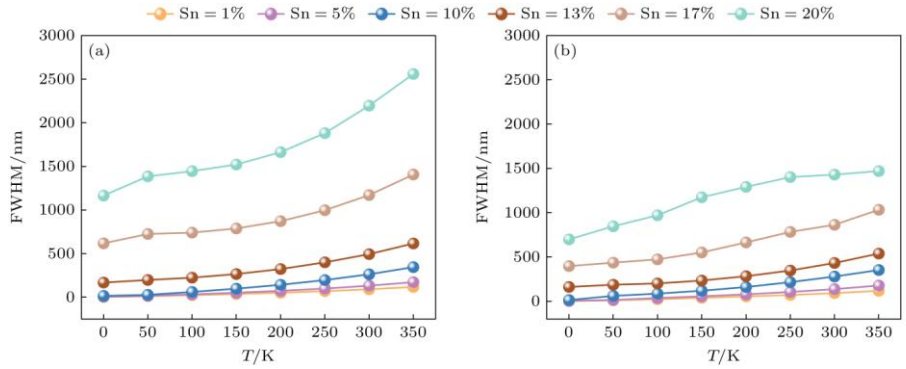

Fig. 6 Temperature dependence of the full width at half maximum (FWHM) of spontaneous emission spectra of GeSn alloys: (a) Thermal excitation model; (b) phonon-assisted model.

Figure 7 illustrates the temperature-dependent shift in peak positions of the spontaneous emission spectra of GeSn alloys with varying Sn compositions. Under both models, a redshift in peak position intensifies with increasing temperature and higher Sn composition, directly resulting from the bandgap narrowing effect. Furthermore, a comparison between the two models reveals that, for high-Sn-composition GeSn alloys at elevated temperatures, the phonon-assisted model predicts a significantly larger redshift than the thermal excitation model. This discrepancy arises because electron-phonon coupling more readily induces band renormalization at high temperatures, leading to additional bandgap contraction.

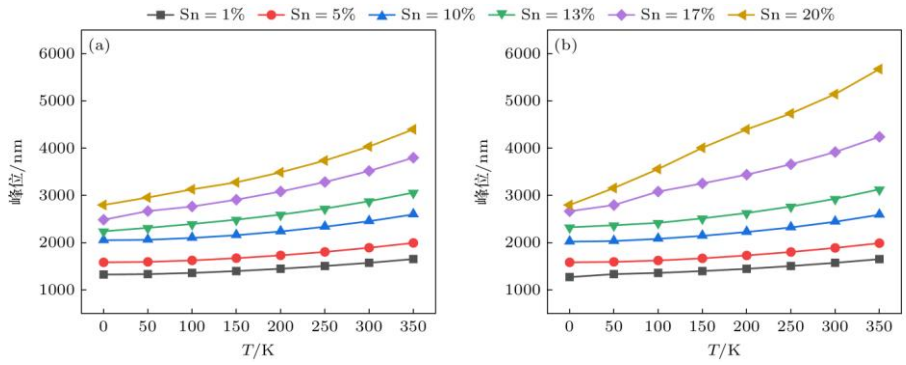

Fig. 7 Variation of emission peak energy with temperature for GeSn alloys under (a) thermal excitation and (b) phonon-assisted models.

4 Conclusion

This study constructs a theoretical model incorporating band parameters, nonequilibrium carrier transport, and radiative recombination to systematically elucidate the regulatory mechanisms of thermal excitation and phonon-assisted processes on the temperature-dependent spontaneous emission in GeSn alloys.

Compared with prior literature, this work quantitatively characterizes the synergistic role of thermal excitation and phonon assistance in the bidirectional competition between carrier injection and escape, thereby deepening the microscopic understanding of carrier dynamics. The main conclusions are as follows: Composition-dependent valley carrier transfer characteristics. In low-composition GeSn alloys with Sn content below 10%, thermally induced electron transfer from the L_{CBM} to the Γ_{CBM} dominates, leading to enhanced direct-band emission efficiency with increasing temperature. In high-composition GeSn alloys with Sn content between 10% and 20%, electron escape from the Γ_{CBM} to the L_{CBM} becomes significantly pronounced, resulting in reduced direct-band emission efficiency as temperature rises. 2) Competition mechanism between carrier transport and radiative recombination. An improved Arrhenius model demonstrates that thermal excitation and phonon assistance exert bidirectional regulatory effects on electron injection into or escape from the Γ_{CBM}. In low-composition alloys, phonon assistance promotes electron injection from the L_{CBM} into the Γ_{CBM} more effectively than thermal excitation alone, thereby enhancing direct-band radiative recombination. In high-composition alloys, phonon assistance further drives electron escape from the Γ_{CBM} to the L_{CBM}, becoming a critical factor limiting the direct-band emission efficiency of GeSn alloys. 3) Influence of phonon-assisted processes on emission peak position and full width at half maximum (FWHM). The emission peak of the spontaneous emission spectrum in GeSn alloys exhibits a redshift with increasing temperature and Sn composition, primarily due to bandgap narrowing. Phonon-involved processes reduce the energy dispersion of carriers, leading to a pronounced spectral narrowing effect in the spontaneous emission lineshape. The findings of this study not only advance the quantitative understanding of spontaneous emission mechanisms in GeSn alloys but also provide crucial theoretical support for band structure engineering and emission efficiency optimization in optoelectronic devices such as photodetectors and lasers based on these materials.

References

[1] Chang G E, Yu S Q, Liu J, Cheng H H, Soref R A, Sun G 2022 *IEEE J. Sel. Topics Quantum Electron.* **28** 3800611

[2] Giunto A, Morral A F I 2024 *Appl. Phys. Rev.* **11** 41333

[3] An S, Park H, Kim M 2023 *J. Mater. Chem. C* **11** 2430

[4] Miao Y H, Wang G L, Kong Z Z, Xu B Q, Zhao X W, Luo X, Lin H X, Dong Y, Lu B, Dong L P, Zhou J R, Liu J B, Radamson H H 2021 *Nanomaterials* **11** 2556

[5] Reboud V, Gassenq A, Pauc N, Aubin J, Milord L, Thai Q M, Bertrand M,

Guilloy K, Rouchon D, Rothman J, Zabel T, Armand P F, Sigg H, Chelnokov A, Hartmann J M, Calvo V 2017 *Appl. Phys. Lett.* **111** 92101

[6] Ghosh S, Bansal R, Sun G, Soref R A, Cheng H H, Chang G E 2022 *Sensors* **22** 3978

[7] Huang Y P, Wu B R, Ghosh S, Jheng Y T, Ho Y L, Wu Y J, Wisessint A, Kim M, Chang G E 2024 *Opt. Express* **32** 39560

[8] Qian L, Fan W J, Tan C S, Zhang D H 2017 *Opt. Mater. Express* **7** 800

[9] Liu J F 2014 *Photonics* **1** 162

[10] Sun X, Liu J, Kimerling L C, Michel J 2009 *Appl. Phys. Lett.* **95** 011911

[11] Du W, Ghetmiri S A, Conley B R, Mosleh A, Nazzal A, Soref R A, Sun G, Tolle J, Margetis J, Naseem H A, Yu S Q 2014 *Appl. Phys. Lett.* **105** 51104

[12] Huang S H, Zheng Q Q, Xie W M, Lin J Y, Huang W, Li C, Qi D F 2018 *J. Phys.: Condens. Matter.* **30** 465701

[13] Ryu M Y, Harris T R, Yeo Y K, Beeler R T, Kouvetakis J 2013 *Appl. Phys. Lett.* **102** 171908

[14] Julsgaard B, Von D, Tidemand L P, Pedersen C, Ikonic Z, Buca D 2020 *Photonics Res.* **8** 788

[15] Menéndez J, Poweleit C D, Tilton S E 2020 *Phys. Rev. B* **101** 195204

[16] Wu S S, Huang S H, Qian J H, Huang W, Lin G Y, Cheng S Y, Li C 2025 *J. Phys. D: Appl. Phys.* **58** 135308

[17] Viña L, Logothetidis S, Cardona M 1984 *Phys. Rev. B* **30** 1979

[18] Bertrand M, Thai Q, Chrétien J, Pauc N, Aubin J, Milord L, Gassenq A, Hartmann J, Chelnokov A, Calvo V, Reboud V 2019 *Annal. Phys.* **531** 1800396

[19] Hong H Y, Zhang L, Qian K, An Y Y, Li C, Li J, Chen S Y, Huang W, Wang J Y, Zhang S H 2021 *Opt. Express* **29** 441

[20] Huang S H, Li J P, Li H L, Lu X X, Sun Q Q, Xie D 2025 *Acta Phys. Sin.* **74** 36101

[21] Huang S H, Li C, Chen C Z, Zheng Y Y, Lai H K, Chen S Y 2012 *Acta Phys. Sin.* **61** 36202 (in Chinese)

[22] Chuang S L 2009 *Physics of Photonic Devices* 2nd ed (Hoboken, N. J: John Wiley & Sons) p347

[23] Wirths S, Geiger R, Von Den Driesch N, Mussler G, Stoica T, Mantl S, Ikonic Z, Luysberg M, Chiussi S, Hartmann J M, Sigg H, Faist J, Buca D, Grützmacher D 2015 *Nat. Photonics* **9** 88

[24] Ghosh S, Sun G, Yu S Q, Chang G E 2025 *IEEE J. Select. Topics Quantum Electron.* **31** 1

[25] Huang B J, Chang C Y, Hsieh Y D, Soref R A, Sun G, Cheng H H, Chang G

E 2019 *ACS Photonics* **6** 1931
[26]Huang Q X, Liu X Q, Zheng J, Yang Y Z, Zhang D D, Pang Y Q, Cui J L, Liu Z, Zuo Y H, Cheng B W 2023 *J. Lumin.* **255** 119623
[27]Fang Y T, Wang L, Sun Q L, Lu T P, Deng Z, Ma Z G, Jiang Y, Jia H Q, Wang W X, Zhou J M, Chen H 2015 *Sci. Rep.* **5** 12718